JACS
JOURNAL OF THE AMERICAN CHEMICAL SOCIETY

pubs.acs.org/JACS

Communication

Renal-Clearable Molecular Probe for Near-Infrared Fluorescence Imaging and Urinalysis of SARS-CoV-2

Si Si Liew,[†] Ziling Zeng,[†] Penghui Cheng, Shasha He, Chi Zhang, and Kanyi Pu*

Cite This: https://doi.org/10.1021/jacs.1c08017

Read Online

ACCESS | Metrics & More | Article Recommendations | Supporting Information

ABSTRACT: Despite the importance of rapid and accurate detection of SARS-CoV-2 in controlling the COVID-19 pandemic, current diagnostic methods are static and unable to distinguish between viable/nonviable virus or directly reflect viral replication activity. Real-time imaging of protease activity specific to SARS-CoV-2 can overcome these issues but remains lacking. Herein, we report a near-infrared fluorescence (NIRF) activatable molecular probe (SARS-CyCD) for detection of SARS-CoV-2 protease in living mice. The probe comprises a hemicyanine fluorophore caged with a protease peptide substrate and a cyclodextrin unit, which function as an NIRF signaling moiety and a renal-clearable enabler, respectively. The peptide substrate of SARS-CyCD can be specifically cleaved by SARS-CoV-2 main protease (M^{pro}), resulting in NIRF signal activation and liberation of the renal-clearable fluorescent fragment (CyCD). Such a design not only allows sensitive detection of M^{pro} in the lungs of living mice after intratracheal administration but also permits optical urinalysis of SARS-CoV-2 infection. Thus, this study presents an in vivo sensor that holds potential in preclinical high-throughput drug screening and clinical diagnostics for respiratory viral infections.

The emergence of SARS-CoV-2 has brought about a global pandemic with huge societal and economic repercussions.[1] As the symptoms of coronavirus disease 2019 (COVID-19) closely resemble the common flu and seasonal upper respiratory tract infections, precise diagnostic tests are crucial for rapid detection of SARS-CoV-2.[2] Real-time polymerase chain reaction (RT-PCR) is the gold standard for identifying active infections via detecting SARS-CoV-2 ribonucleic acids with high sensitivity and selectivity.[2,3] Antigen-rapid tests (ARTs) are developed as point-of-care tests to detect ongoing COVID-19 infections; however, the high risks of false negative results render them complementary to RT-PCR.[4,5] Serological tests are useful for staging past infections by quantifying host IgM/IgG antibodies levels against viral proteins. However, these diagnostic methods are static and unable to distinguish between viable/nonviable virus or reflect viral replication activity.[6] Thereby, multiple patient sample collections are required to monitor the clinical phases of infection. Despite the recent growing body of available and in-development diagnostics,[7−11] approaches for real-time, dynamic imaging of SARS-CoV-2 remain inchoate.

Molecular optical probes that activate their signals in the presence of biomarkers are powerful tools for real-time noninvasive imaging of diseases in vivo.[12−15] Although fluorescence molecular probes have been widely applied to detect proteases for diagnosis of kidney/liver injury,[16−18] cancer,[19−21] inflammation,[22] and neurodegenerative diseases,[23,24] they have been less exploited for virus detection.[25,26] A few examples include detection of dengue virus,[27] human immunodeficiency virus (HIV),[28] and SARS-CoV-2 virus.[29,30] However, they are limited to in vitro studies because of the shallow tissue-penetrating wavelengths of these probes. Considering the potential advantages in direct monitoring of viral replication activity, clinicopathologic staging of infection, and high-throughput inhibitor screening, fluorescence molecular probes capable of real-time dynamic in vivo imaging of SARS-CoV-2 are highly desired.[31,32]

Herein, we report the first protease-activatable near-infrared fluorescence (NIRF) probe (termed SARS-CyCD) for in vivo imaging and urinalysis of SARS-CoV-2. The main protease (M^{pro}), one of the key coronavirus proteases in viral polypeptide processing,[33] was chosen as the biomarker for signal activation of SARS-CyCD.[18] M^{pro} has also been validated as an in vivo diagnostic marker for SARS-CoV-2.[29,30] SARS-CyCD comprises a hemicyanine fluorophore caged with the M^{pro} peptide substrate (*N*-Acetyl-Abu-Tle-Leu-Gln(Trt)−OH) via a *para*-aminobenzylalcohol (PABA) self-immolative linker (Scheme 1). The hemicyanine fluorophore and cyclodextrin function as a NIRF signaling moiety and renal-clearance enabler, respectively. After intratracheal (i.t.) administration into the lungs of living mice, the peptide substrate of SARS-CyCD is cleaved by SARS-CoV-2 M^{pro}, resulting in NIRF "Turn-ON" and the release of the fluorescent fragment CyCD. Because of the high renal clearance, CyCD can be excreted into urine for sensitive urinalysis of SARS-CoV-2. Such a delivery strategy enables the probe to avoid the first-pass metabolism with good bioavailability in the lungs, the main route of viral entry where viral load is high.[34] Subsequent in vivo NIRF imaging of the lungs and optical urinalysis can therefore permit non-

Received: August 2, 2021

Scheme 1. Scheme Depicting In Vivo Detection of SARS-CoV-2 via i.t. Injection of M^{pro}-Activatable NIRF Probe (SARS-CyCD), Followed by NIRF Imaging and Optical Urinalysis; Lower Right: Chemical Structure of SARS-CyCD (R = H or 2-Hydroxylpropyl) and Its Activated Form, CyCD, in Response to M^{pro}

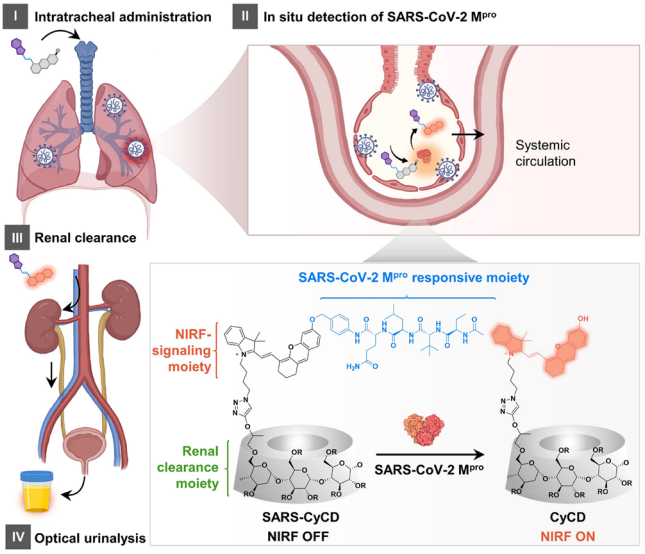

invasive and real-time detection of SARS-CoV-2 (Scheme 1), further highlighting its potential for clinical translation.

SARS-CyCD was prepared as shown in Scheme S1. First, SARS-CoV-2 peptide substrate (SARS(Trt), *N*-Acetyl-Abu-Tle-Leu-Gln(Trt)−OH)[29] was synthesized using standard solid-phase peptide synthesis, followed by amide coupling with PABA to yield SARS(Trt)-PABA. Next, SARS(Trt)-PABA was brominated using PBr_3, followed by nucleophilic substitution with CyOH to obtain compound SARS(Trt)-Cy. Removal of the trityl (Trt) protecting group with trifluoroacetic acid afforded SARS-Cy. Finally, copper(I)-catalyzed alkyne−azide cycloaddition (CuAAC) reaction of SARS-Cy with propynyl-HPβCD afforded SARS-CyCD.

The in vitro response of SARS-CyCD toward SARS-CoV-2 M^{pro} was studied. First, the optical properties were examined with and without SARS-CoV-2 M^{pro}. SARS-CyCD showed two characteristic UV absorption peaks at 625 and 680 nm and was initially nonfluorescent when caged with the peptide substrate (Figure 1a,b). After incubation with SARS-CoV-2 M^{pro}, the absorption peak at 625 nm disappeared, and a new peak appeared at 690 nm (Figure 1a). In Figure 1b, fluorescence measurements indicated a 50-fold fluorescence "Turn-ON" enhancement at 710 nm, with the successful uncaging of SARS-CyCD. High-performance liquid chromatography (HPLC) analysis confirmed the release of CyCD (t_R = 18 min) in the presence of SARS-CoV-2 M^{pro} (Figure 1c). The enzymatic Michaelis−Menten constant (K_m) of SARS-CoV-2 M^{pro} toward SARS-CyCD was calculated to be 11.5 μM (Figure 1d). The catalytic rate constant (k_{cat}) of SARS-CoV-2 M^{pro} toward SARS-CyCD was 0.014 s^{-1}, whereas the catalytic efficiency (k_{cat}/K_m) of SARS-CoV-2 M^{pro} toward SARS-CyCD was determined to be 12.2 × 10^6 M^{-1} s^{-1}. More importantly, the NIRF intensity of SARS-CyCD did not show any significant increase when incubated with other enzymes, suggesting its high specificity toward SARS-CoV-2 M^{pro} (Figure 1e,f).

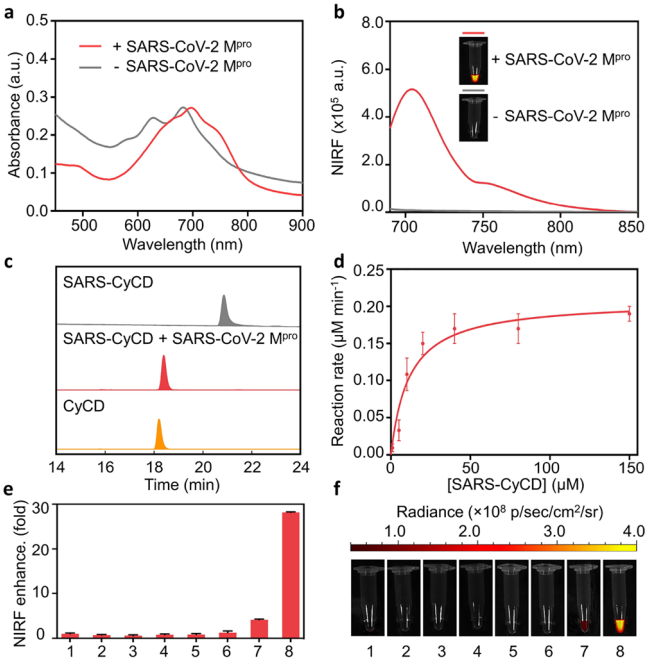

Figure 1. In vitro characterization of SARS-CyCD. (a) UV/vis absorption spectra and (b) fluorescence spectra of SARS-CyCD (10 μM) after incubation with/without SARS-CoV-2 M^{pro} (250 nM) in Tris buffer (20 mM, pH 7.4) at 37 °C. (c) HPLC spectra of SARS-CyCD (10 μM) after incubation with/without SARS-CoV-2 M^{pro} (250 nM). (d) Nonlinear regression analysis of SARS-CyCD cleavage rate, V (μM min^{-1}), as a function of substrate concentration. SARS-CyCD (1, 5, 10, 20, 40, 80, 150 μM) was incubated with SARS-CoV-2 M^{pro} (250 nM) at 37 °C for 30 min in Tris buffer (20 mM, pH 7.4), followed by HPLC measurement. (e) NIRF enhancement and (f) the corresponding images after SARS-CyCD (10 μM) was incubated with different enzymes (250 nM) at 37 °C for 120 min. 1, blank; 2, HCV NS4A/NS3−3 protease; 3, urokinase; 4, caspase-3; 5, furin; 6, GGT; 7, SARS-CoV-1 M^{pro}; 8, SARS-CoV-2 M^{pro}. Error bars: standard deviation from three separate measurements.

The pharmacokinetics of SARS-CyCD was investigated along with its uncaged fragment (CyCD). After intratracheal (i.t.) injection, SARS-CyCD or CyCD concentrations in plasma were analyzed. At 110 min postinjection, CyCD concentration in plasma reached 0% of the injected dose (ID), with an elimination half-life ($t_{1/2}$) of 37−39 min; SARS-CyCD had a slower elimination (180 min) with a $t_{1/2}$ of approximately 52−54 min (Figure 2a). The renal clearance efficiencies (RCE) of both SARS-CyCD and CyCD were determined by fluorescence quantification of CyCDs in the urine collected from living mice as a function of time after i.t. injection. Following 24 h postinjection, the RCE of SARS-CyCD was determined to be 59 ± 5.0% ID, lower than that of CyCD (79 ± 1.5% ID) (Figure 2b). This was attributed to the higher hydrophilicity of CyCD with a lower Log *D* value (Table S1) relative to SARS-CyCD because of the hydrophobic peptide moiety.

Next, the in vivo stability of SARS-CyCD was investigated by NIRF imaging and fluorescence measurements of SARS-CyCD recovered from urine. Compared to CyCD, negligible fluorescence "Turn-ON" was observed for excreted SARS-CyCD (Figure S2a). Furthermore, excreted SARS-CyCD showed almost identical fluorescence as the reference in PBS (Figure S2b). In Figure 2c, HPLC analysis of SARS-CyCD also showed an almost identical profile with the reference

https://doi.org/10.1021/jacs.1c08017
J. Am. Chem. Soc. XXXX, XXX, XXX−XXX

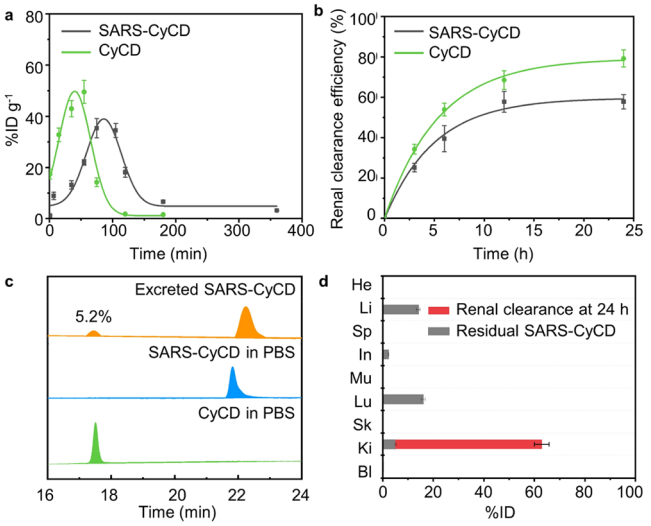

Figure 2. Renal clearance and in vivo stability studies of SARS-CyCD. (a) Plasma concentration (% ID g^{-1}) of SARS-CyCD determined by fluorescence measurements after i.t. injection into living mice. (b) Renal clearance efficiency (RCE) determined by fluorescence measurements post i.t. injection of SARS-CyCD (2 μmol kg^{-1} body weight) in living mice. (c) In vivo stability studies of SARS-CyCD via HPLC analysis of excreted components in urine samples after i.t. administration. (d) RCE of SARS-CyCD at 24 h after i.t. administration. Heart (He), liver (Li), spleen (Sp), intestine (In), muscle (Mu), lung (Lu), skin (Sk), kidney (Ki), and bladder (Bl). Error bars: standard deviation from three separate measurements.

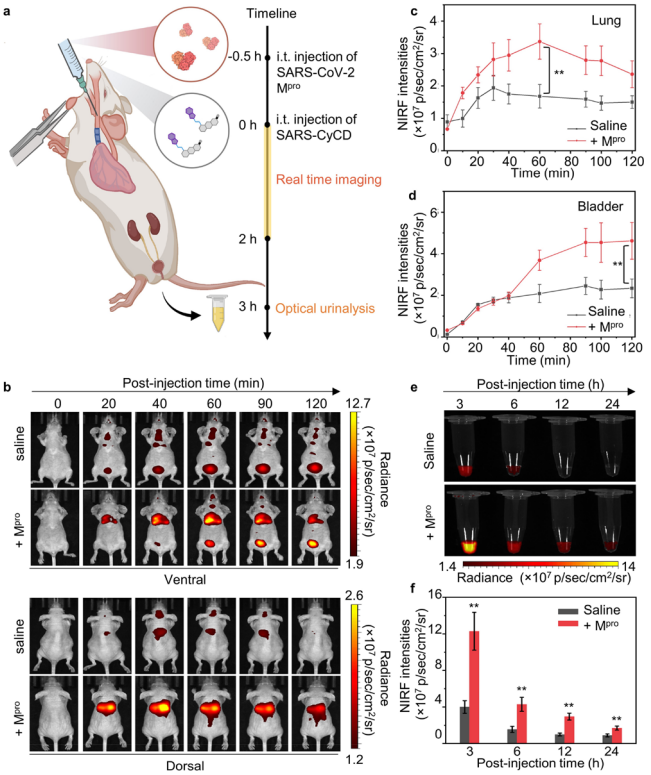

Figure 3. (a) Timeline for i.t. injection of SARS-CoV-2 M^{pro} and SARS-CyCD, followed by NIRF imaging and optical urinalysis. (b) NIRF images at 0, 20, 40, 60, 90, and 120 min after i.t. injection of 0.15 mg kg^{-1} SARS-CoV-2 M^{pro} and 2 μmol kg^{-1} SARS-CyCD into living mice. Dynamic NIRF intensities of (c) lungs (ventral) and (d) bladder as a function of time postinjection of SARS-CyCD in living mice. (e) Fluorescence images and (f) enhancement of excreted SARS-CyCD or CyCD in the urine of living mice collected at different time points post i.t. injection. The values relative to the control groups, where $^{**}p < 0.01$ ($n = 3$).

compound in PBS. Together, these data confirmed that SARS-CyCD underwent negligible in vivo metabolism in living mice. After 24 h urinary recovery, residual SARS-CyCD in the body was determined. The mice were dissected, followed by homogenization of major organs in PBS. Extraction of SARS-CyCD from each organ and subsequent analysis were conducted. Residual SARS-CyCD mainly accumulated in the lungs (ca. 16% ID), liver (ca. 14% ID), and kidneys (ca. 5% ID). In the other organs, negligible amounts of SARS-CyCD were found (Figure 2d).

Because of a lack of established mouse models for studying SARS-CoV-2 lung infection, the potential of SARS-CyCD for in vivo detection of SARS-CoV-2 was validated in an artificial SARS-CoV-2 M^{pro}-positive mice model established via i.t. injection of commercially available recombinant SARS-CoV-2 M^{pro} as proof-of-concept (Figure 3a). After 0.5 h injection of the protease, SARS-CyCD was administered via i.t. injection. At different time points, whole-body longitudinal NIRF imaging of the mice was conducted. Strong NIRF signals were observed in the lungs (both dorsal and ventral views) of SARS-CoV-2 M^{pro}-positive mice (Figure 3b). As for the control group without SARS-CoV-2 M^{pro}, negligible NIRF signals were observed. NIRF signals in the lungs of SARS-CoV-2 M^{pro}-positive mice further increased by up to 5.0-fold (ventral) and 7.5-fold (dorsal) at 60 min post i.t. injection (Figure 3c). However, the negative control group showed only 2.2-fold (ventral) and 3.5-fold (dorsal) increases in NIRF fluorescence intensity (Figure S3a). Furthermore, ex vivo fluorescence analysis of lungs collected from SARS-CoV-2 M^{pro}-positive mice coinjected with saline or SARS-CyCD 24 h post i.t. injection indicated 5-fold enhancement (Figure S3b). These results clearly indicated that cleavage of SARS-CyCD occurred in SARS-CoV-2 M^{pro}-positive mice, giving rise to a gradual increase in NIRF "Turn-ON" signals from uncaged CyCD.

At 60 min postinjection of SARS-CyCD, NIRF imaging easily delineated the bladder because of fast and efficient renal clearance of the cleaved product (CyCD) (Figure 3b). Note that the bladders of the control mice had negligible NIRF signals (Figure 3b). Furthermore, a 2.2-fold increase in NIRF fluorescence intensity was observed in the bladders of SARS-CoV-2 M^{pro}-positive mice compared to saline-treated control (Figure 3d). Optical urinalysis was also carried out by fluorescence measurement of SARS-CyCD in the urine of mice at various time points after i.t. injection. The NIRF signal for the urine of SARS-CoV-2 M^{pro}-positive mice was higher than that of mice in the control group at all time points. In particular, a 3.0-fold maximum significant NIRF difference relative to the control group was observed 3 h post i.t. injection (Figure 3e,f). Thus, SARS-CyCD-based optical urinalysis was validated as a potential method for specific detection of SARS-CoV-2 infection.

In conclusion, we have developed a M^{pro}-activatable NIRF probe (SARS-CyCD) for in vivo detection of SARS-CoV-2. Our in vitro results demonstrated that this probe is specifically activated in the presence of SARS-CoV-2 M^{pro} for fluorescence signal "Turn-ON". Pharmacokinetics studies indicated that SARS-CyCD has high renal-clearance efficiency and minimal in vivo metabolism. Such hemicyanine-based probes have also

https://doi.org/10.1021/jacs.1c08017
J. Am. Chem. Soc. XXXX, XXX, XXX−XXX

been used in animal models and showed no cytotoxicity (Figure S4).[14,8,19] Upon i.t. administration, SARS-CyCD was effectively cleaved by SARS-CoV-2 M^{pro} in the lungs of living mice to liberate its fluorescent fragment (CyCD), followed by excretion via kidneys. Thus, SARS-CyCD can detect SARS-CoV-2 infection through optical urinalysis, showing its high potential for clinical translation.

To the best of our knowledge, this work provides the first example of a fluorescence probe capable of real-time, noninvasive imaging and urinalysis of SARS-CoV-2 infection. As it detects viral protease, this approach holds potential for directly monitoring viral replication activity during infection, unlike current in vitro diagnostic methods, which are static. Although i.t. administration was applied in this study, SARS-CyCD can be further developed into aerosols with the assistance of ventilators, aerosolizers, or portable nebulizers, allowing for convenient administration via inhalation. Thus, we envision that SARS-CyCD may represent a new generation of inhalation-based urine tests for COVID-19 detection.

■ ASSOCIATED CONTENT

Supporting Information

The Supporting Information is available free of charge at https://pubs.acs.org/doi/10.1021/jacs.1c08017.

Detailed experimental procedures and supporting figures as described in the text (PDF)

■ AUTHOR INFORMATION

Corresponding Author

Kanyi Pu − *School of Chemical and Biomedical Engineering, Nanyang Technological University, Singapore 637457; School of Physical and Mathematical Sciences, Nanyang Technological University, Singapore 637371; Lee Kong Chian School of Medicine, Nanyang Technological University, Singapore 636921;* orcid.org/0000-0002-8064-6009; Email: kypu@ntu.edu.sg

Authors

Si Si Liew − *School of Chemical and Biomedical Engineering, Nanyang Technological University, Singapore 637457*

Ziling Zeng − *School of Chemical and Biomedical Engineering, Nanyang Technological University, Singapore 637457*

Penghui Cheng − *School of Chemical and Biomedical Engineering, Nanyang Technological University, Singapore 637457*

Shasha He − *School of Chemical and Biomedical Engineering, Nanyang Technological University, Singapore 637457*

Chi Zhang − *School of Chemical and Biomedical Engineering, Nanyang Technological University, Singapore 637457*

Complete contact information is available at: https://pubs.acs.org/10.1021/jacs.1c08017

Author Contributions

†S.S.L and Z.Z. contributed equally to this work.

Notes

The authors declare no competing financial interest.

■ ACKNOWLEDGMENTS

K.P. thanks Singapore Ministry of Education, Academic Research Fund Tier 1 (2019-T1-002-045, RG125/19, RT05/20), Academic Research Fund Tier 2 (MOE2018-T2-2-042), and A*STAR SERC AME Programmatic Fund (SERC A18A8b0059) for the financial support.

■ REFERENCES

(1) Hu, B.; Guo, H.; Zhou, P.; Shi, Z. L. Characteristics of SARS-CoV-2 and COVID-19. *Nat. Rev. Microbiol.* **2021**, *19*, 141−154.

(2) Yuan, X.; Yang, C.; He, Q.; Chen, J.; Yu, D.; Li, J.; Zhai, S.; Qin, Z.; Du, K.; Chu, Z.; Qin, P. Current and perspective diagnostic techniques for COVID-19. *ACS Infect. Dis.* **2020**, *6*, 1998−2016.

(3) Habli, Z.; Saleh, S.; Zaraket, H.; Khraiche, M. L. COVID-19 in-vitro diagnostics: state-of-the-art and challenges for rapid, scalable, and high-accuracy screening. *Front. Bioeng. Biotechnol.* **2021**, *8*, 605702.

(4) Wagenhauser, I.; Knies, K.; Rauschenberger, V.; Eisenmann, M.; McDonogh, M.; Petri, N.; Andres, O.; Flemming, S.; Gawlik, M.; Papsdorf, M.; Taurines, R.; Bohm, H.; Forster, J.; Weismann, D.; Weissbrich, B.; Dolken, L.; Liese, J.; Kurzai, O.; Vogel, U.; Krone, M. Clinical performance evaluation of SARS-CoV-2 rapid antigen testing in point of care usage in comparison to RT-qPCR. *EBioMedicine* **2021**, *69*, 103455.

(5) Corman, V. M.; Haage, V. C.; Bleicker, T.; Schmidt, M. L.; Mühlemann, B.; Zuchowski, M.; Jo, W. K.; Tscheak, P.; Möncke-Buchner, E.; Müller, M. A.; Krumbholz, A.; Drexler, J. F.; Drosten, C. Comparison of seven commercial SARS-CoV-2 rapid point-of-care antigen tests: a single-centre laboratory evaluation study. *Lancet Microbe* **2021**, *2*, e311−e319.

(6) Vandenberg, O.; Martiny, D.; Rochas, O.; van Belkum, A.; Kozlakidis, Z. Considerations for diagnostic COVID-19 tests. *Nat. Rev. Microbiol.* **2021**, *19*, 171−183.

(7) Kevadiya, B. D.; Machhi, J.; Herskovitz, J.; Oleynikov, M. D.; Blomberg, W. R.; Bajwa, N.; Soni, D.; Das, S.; Hasan, M.; Patel, M.; Senan, A. M.; Gorantla, S.; McMillan, J.; Edagwa, B.; Eisenberg, R.; Gurumurthy, C. B.; Reid, S. P. M.; Punyadeera, C.; Chang, L.; Gendelman, H. E. Diagnostics for SARS-CoV-2 infections. *Nat. Mater.* **2021**, *20*, 593−605.

(8) Tang, Z.; Kong, N.; Zhang, X.; Liu, Y.; Hu, P.; Mou, S.; Liljestrom, P.; Shi, J.; Tan, W.; Kim, J. S.; et al. A materials-science perspective on tackling COVID-19. *Nat. Rev. Mater.* **2020**, *5*, 1−14.

(9) Iravani, S. Nano- and biosensors for the detection of SARS-CoV-2: challenges and opportunities. *Mater. Adv.* **2020**, *1*, 3092−3103.

(10) Ning, B.; Yu, T.; Zhang, S.; Huang, Z.; Tian, D.; Lin, Z.; Niu, A.; Golden, N.; Hensley, K.; Threeton, B.; et al. A smartphone-read ultrasensitive and quantitative saliva test for COVID-19. *Sci. Adv.* **2021**, *7*, No. eabe3703.

(11) Ning, B.; Huang, Z.; Youngquist, B. M.; Scott, J. W.; Niu, A.; Bojanowski, C. M.; Zwezdaryk, K. J.; Saba, N. S.; Fan, J.; Yin, X. M.; Cao, J.; Lyon, C. J.; Li, C. Z.; Roy, C. J.; Hu, T. Y. Liposome-mediated detection of SARS-CoV-2 RNA-positive extracellular vesicles in plasma. *Nat. Nanotechnol.* **2021**, *16*, 1039−1044.

(12) Wu, L.; Huang, J.; Pu, K.; James, T. D. Dual-locked spectroscopic probes for sensing and therapy. *Nat. Rev. Chem.* **2021**, *5*, 406−421.

(13) Cheng, P.; Pu, K. Molecular imaging and disease theranostics with renal-clearable optical agents. *Nat. Rev. Mater.* **2021**, DOI: 10.1038/s41578-021-00328-6.

(14) Zeng, Z.; Liew, S. S.; Wei, X.; Pu, K. Hemicyanine-based near-infrared activatable probes for imaging and diagnosis of diseases. *Angew. Chem., Int. Ed.* **2021**, DOI: 10.1002/anie.202107877.

(15) Ye, S.; Hananya, N.; Green, O.; Chen, H.; Zhao, A. Q.; Shen, J.; Shabat, D.; Yang, D. A highly selective and sensitive chemiluminescent probe for real-time monitoring of hydrogen peroxide in cells and animals. *Angew. Chem., Int. Ed.* **2020**, *59*, 14326−14330.

(16) Cheng, P.; Miao, Q.; Huang, J.; Li, J.; Pu, K. Multiplex optical urinalysis for early detection of drug-induced kidney injury. *Anal. Chem.* **2020**, *92*, 6166−6172.

(17) Chen, J.; Fang, Y.; Sun, L.; Zeng, F.; Wu, S. An activatable probe for detecting alcoholic liver injury via multispectral optoacoustic tomography and fluorescence imaging. *Chem. Commun.* **2020**, *56*, 11102−11105.

(18) Huang, J.; Li, J.; Lyu, Y.; Miao, Q.; Pu, K. Molecular optical imaging probes for early diagnosis of drug-induced acute kidney injury. *Nat. Mater.* **2019**, *18*, 1133−1143.
(19) Huang, J.; Jiang, Y.; Li, J.; He, S.; Huang, J.; Pu, K. A renal-clearable macromolecular reporter for near-infrared fluorescence imaging of bladder cancer. *Angew. Chem., Int. Ed.* **2020**, *59*, 4415−4420.
(20) Wang, R.; Chen, J.; Gao, J.; Chen, J. A.; Xu, G.; Zhu, T.; Gu, X.; Guo, Z.; Zhu, W. H.; Zhao, C. A molecular design strategy toward enzyme-activated probes with near-infrared I and II fluorescence for targeted cancer imaging. *Chem. Sci.* **2019**, *10*, 7222−7227.
(21) Li, H.; Kim, D.; Yao, Q.; Ge, H.; Chung, J.; Fan, J.; Wang, J.; Peng, X.; Yoon, J. Activity-based NIR enzyme fluorescent probes for the diagnosis of tumors and image-guided surgery. *Angew. Chem., Int. Ed.* **2021**, *60*, 17268−17289.
(22) Fernandez, A.; Vendrell, M. Smart fluorescent probes for imaging macrophage activity. *Chem. Soc. Rev.* **2016**, *45*, 1182−1196.
(23) Gardner, S. H.; Brady, C. J.; Keeton, C.; Yadav, A. K.; Mallojjala, S. C.; Lucero, M. Y.; Su, S.; Yu, Z.; Hirschi, J. S.; Mirica, L. M.; Chan, J. A general approach to convert hemicyanine dyes into highly optimized photoacoustic scaffolds for analyte sensing. *Angew. Chem., Int. Ed.* **2021**, *60*, 18860−18866.
(24) Zhou, J.; Jangili, P.; Son, S.; Ji, M. S.; Won, M.; Kim, J. S. Fluorescent diagnostic probes in neurodegenerative diseases. *Adv. Mater.* **2020**, *32*, No. e2001945.
(25) Sewald, X. Visualizing viral infection in vivo by multi-photon intravital microscopy. *Viruses* **2018**, *10*, 337.
(26) Hofherr, S. E.; Adams, K. E.; Chen, C. Y.; May, S.; Weaver, E. A.; Barry, M. A. Real-time dynamic imaging of virus distribution in vivo. *PLoS One* **2011**, *6*, No. e17076.
(27) Zhang, S. L.; Tan, H. C.; Hanson, B. J.; Ooi, E. E. A simple method for Alexa Fluor dye labelling of dengue virus. *J. Virol. Methods* **2010**, *167*, 172−177.
(28) Shah, K.; Tung, C.-H.; Chang, C.-H.; Slootweg, E.; O'Loughlin, T.; Breakefield, X. O.; Weissleder, R. In vivo imaging of HIV protease activity in amplicon vector-transduced gliomas. *Cancer Res.* **2004**, *64*, 273−278.
(29) Rut, W.; Groborz, K.; Zhang, L.; Sun, X.; Zmudzinski, M.; Pawlik, B.; Wang, X.; Jochmans, D.; Neyts, J.; Mlynarski, W.; Hilgenfeld, R.; Drag, M. SARS-CoV-2 M(pro) inhibitors and activity-based probes for patient-sample imaging. *Nat. Chem. Biol.* **2021**, *17*, 222−228.
(30) Alhadrami, H. A.; Hassan, A. M.; Chinnappan, R.; Al-Hadrami, H.; Abdulaal, W. H.; Azhar, E. I.; Zourob, M. Peptide substrate screening for the diagnosis of SARS-CoV-2 using fluorescence resonance energy transfer (FRET) assay. *Microchim. Acta* **2021**, *188*, 137.
(31) Maddali, H.; Miles, C. E.; Kohn, J.; O'Carroll, D. M. Optical Biosensors for Virus Detection: Prospects for SARS-CoV-2/COVID-19. *ChemBioChem* **2021**, *22*, 1176−1189.
(32) Cordon-Cardo, C.; Pujadas, E.; Wajnberg, A.; Sebra, R.; Patel, G.; Firpo-Betancourt, A.; Fowkes, M.; Sordillo, E.; Paniz-Mondolfi, A.; Gregory, J.; Krammer, F.; Simon, V.; Isola, L.; Soon-Shiong, P.; Aberg, J. A.; Fuster, V.; Reich, D. L. COVID-19: Staging of a new disease. *Cancer Cell* **2020**, *38*, 594−597.
(33) V'Kovski, P.; Kratzel, A.; Steiner, S.; Stalder, H.; Thiel, V. Coronavirus biology and replication: implications for SARS-CoV-2. *Nat. Rev. Microbiol.* **2021**, *19*, 155−170.
(34) Anselmo, A. C.; Gokarn, Y.; Mitragotri, S. Non-invasive delivery strategies for biologics. *Nat. Rev. Drug Discovery* **2019**, *18*, 19−40.

https://doi.org/10.1021/jacs.1c08017
J. Am. Chem. Soc. XXXX, XXX, XXX−XXX